

# NUCLEATION RATES OF WATER USING STATISTICAL ASSOCIATION FLUID THEORY

Fawaz Hrahsheh<sup>1, a)</sup>

Faculty of Engineering Technology and Science, Higher Colleges of Technology, MZWC, Abu Dhabi 58855, UAE

(Dated: 15 December 2024)

The SAFT-0 is an equation of state (EOS) that considers the effects of molecular association based on the statistical association fluid theory (SAFT). This EOS recently showed relatively successful calculations of the phase-equilibrium properties and the classical and nonclassical nucleation rates of methanol. Motivated by methanol results, we use the SAFT-0 EOS for water, in particular within the temperature range of anomalous density behavior below  $T_{max} = 277.15K$ . To do so, the effective temperature-dependent hard sphere diameter was adjusted for the SAFT-0 EOS in a way that it reproduces the water vapor-liquid equilibria and the vapor pressures, particularly in the temperature range of homogeneous nucleation of water. The Gibbsian form of classical nucleation theory (CNT) (known as the P-form) and nonclassical gradient theory (GT) calculations were carried out using the SAFT-0 EOS with and without including this adjusted diameter. Calculated rates were compared to the experimental values of Wölk and Strey [*J. Phys. Chem. B* 2001, **105**, 11683-11701]. In addition to the phase-equilibrium properties, this adjustment improved the nucleation rates from both GT and CNT by factors of 500 and 100, respectively. To explore this further, the GT and experimental rates were analyzed using Hale's scaled model [*J. Chem. Phys.*, 2005, **122**, 204509]. This analysis shows that the predictions of GT scale relatively well with those of the experimental data.

## I. INTRODUCTION

First-order phase transitions play an important role in science and nature as well as in many technical applications. Simple examples are condensation, evaporation, crystallization, and melting. These first-order phase transitions need to overcome an energy barrier, which is the work of formation of a small embryo or nucleus of the new phase, which emerges from fluctuations within a "supersaturated" mother phase. This initiating process of most first-order phase transitions is called nucleation. The hallmark of such a transition is the discontinuous change of density, for example, the condensation of supersaturated vapor into liquid droplets. Theoretical analysis of nucleation rates is of great importance in connection with atmospheric aerosol formation and materials synthesis, clustering and condensation in vapors, crystallization of liquid alloys, phase separation in solid solutions, kinetics of colloidal and biological systems and many other growth-related phenomena such as thin film condensation, epitaxy of semiconductor quantum dots and freestanding nanowires.

One of the simplest examples to illustrate the mechanism of nucleation is the formation of a small liquid droplet in a supersaturated vapor. If we compress a vapor at constant temperature, the condensation will not commence at the saturation pressure, but above it: the vapor remains in a metastable state for some time until thermal fluctuations form a sufficiently large cluster or nucleus, which can grow spontaneously. Central to nucleation theory is the expression for nucleus (critical-size nanodroplet for spontaneous growing) work of formation. In the 1870s Gibbs<sup>1</sup> showed that this reversible work equals the difference between the free energy

of the metastable phase with and without the droplet present. This macroscopic change of free energy associated with the formation of a nucleus consisting of monomers always contains a volume term and a surface energy term.

The classical nucleation theory originated with the work of Volmer and Weber<sup>2</sup> in 1926. By using the kinetic theory of gases and equilibrium thermodynamics, they derived an expression for the nucleation rates. Farkas<sup>3</sup> (1927), Becker-Döring<sup>4</sup> (1935), Frenkel<sup>5</sup> (1939) and Zeldovich<sup>6</sup> (1942) established the steady-state version of the so-called classical nucleation theory (CNT). The CNT considers the droplet as a uniform bulk phase separated by a sharp interface from the old phase (metastable vapor). The distinct feature of this theory is that it needs experimentally accessible bulk thermodynamic properties to calculate the nucleation rates.

Calculations of the nucleation rate  $J$  are based on the so-called Becker-Döring<sup>4</sup> expression. They assumed that during nucleation, a cluster grows by gaining a molecule at a rate known as the nucleation (or condensation) rate. However, most experiments show that the classically calculated nucleation rates have an incorrect temperature dependence and poor agreement with the observed ones.<sup>7-9</sup> Nonclassical nucleation theories using the density functional theory (DFT)<sup>10</sup> and the gradient theory (GT)<sup>11</sup>, an approximation of DFT, predict a  $T$ -dependence in good agreement with experiment. Instead of the sharp discontinuity of density in the classical nucleation theory (CNT), DFT treats the droplet as a non-uniform system whose density varies continuously with distance from the center of the droplet, eventually reaching the value of the surrounding mother phase.

Nucleation, as the first stage, determines many important properties of the newly forming phase such as the number density, and the size distribution of the nuclei. We need to understand the nucleation process in order to control these parameters in experiments or technical applications. For in-

<sup>a)</sup>Electronic mail: [fyh44f@mst.edu](mailto:fyh44f@mst.edu).

stance, the number and size of nucleating water droplets has an impact on the efficiency and lifetime of a steam turbine as well as the color and reflectivity of clouds, which influences the greenhouse effect.

A previous calculation applied to water using the cubic perturbed hard body (CPHB) improved the predicted nucleation rate values by several orders of magnitudes compared to CNT but it failed to improve the predicted temperature dependence of the rates.<sup>11</sup> On the other hand, GT and CNT calculations using the statistical association fluid theory SAFT-0 EOS<sup>12</sup> were applied to the methanol (another associating vapor).<sup>13,14</sup> The semi-empirical Hale model<sup>15–17</sup> of nucleation rate shows that the methanol rate data exhibit anomalous  $S - T$  dependence while the GT rates using SAFT-0 EOS scale remarkably well, illustrating that the Hale plot can be used to assess the theoretical results and the experimental data, as well.

In this paper, we adjust the prerequisites of the SAFT-0 EOS in a way that it reproduces the vapor pressures and the anomalous water binodal lines below  $T_{max} = 277.15K$  in a good agreement with the experimental data.<sup>18</sup> Moreover, we apply the GT and CNT to water using SAFT-0 EOS to see if this adjustment will yield improved rates predictions in the temperature range where most of the nucleation rates were measured.<sup>8,19</sup>

## II. THEORY

The reversible work  $W$  needed to create a critical-size cluster of the new phase in a metastable vapor is given by Gibbs<sup>1</sup> as:

$$W = A\gamma - V(P_l - P_v). \quad (1)$$

Here,  $A$  and  $\gamma$  are the surface area and surface tension of the droplet, respectively,  $V$  is its volume,  $P_l$  and  $P_v$  are the internal pressure of the droplet (reference pressure) and the actual pressure of the mother phase, respectively, at the same value of the chemical potential for both phases. Using the Laplace equation for the pressure difference between two phases separated by a curved surface, Gibbs<sup>1</sup> found an explicit relation for  $W$  of a critical size droplet as:

$$W = \frac{16\pi}{3} \frac{\gamma_\infty^3}{(P_l - P_v)^2}. \quad (2)$$

Here, the curved surface tension  $\gamma$  is replaced by the experimentally reachable values of flat interfaces  $\gamma_\infty$  because the exact values of  $\gamma$  for typical critical droplets (one nanometer or less radii) are not available. Using this approximation and knowing the reference pressure are the prerequisites for applying the so-called  $P$ -form of work of formation (Equation 2).<sup>11,13</sup>

Calculating the work needed to form the critical-size droplets is the only prerequisite to use the Becker-Döring<sup>4</sup> expression of nucleation rate at specific temperature  $T$ ,

$$J = J_0 \exp\left(-\frac{W}{K_B T}\right) \quad (3)$$

where  $K_B$  is Boltzmann constant and the pre-exponential factor  $J_0$ , is given as:<sup>11</sup>

$$J_0 = \sqrt{\frac{2\gamma_\infty}{\pi m_v}} v_l \left(\frac{P_v}{K_B T}\right)^2 \quad (4)$$

where  $m_v$  is the mass of a condensable vapor molecule, and  $v_l$  is the molecular volume of the new phase.

The Gibbs' expression of the reversible work  $W$  (i.e. free energy barrier) contains two terms (Eqn. 1): a bulk or volumetric term that thermodynamically stabilizes the droplet, and a surface term that is destabilizing because of the increase of free energy associated with forming new surface. Since the surface term is crucial for using Becker-Döring model of nucleation, Cahn and Hilliard<sup>20</sup> wrote the Helmholtz free energy  $F$  as a functional of the system density  $\rho$  with the square-gradient approximation, first proposed by van der Waals<sup>21</sup>, to account for the inhomogeneous interfacial region separating the critical droplet from the uniform mother phase. Their functional is given by:

$$F[\rho(r)] = \int dr f[\rho(r)] = \int dr (f_0[\rho(r)] + (c/2)[\nabla\rho(r)]^2). \quad (5)$$

Here,  $f$  and  $f_0$  are the Helmholtz free energy densities of the inhomogeneous and homogeneous fluids, respectively, and  $c$  is the so-called influence parameter,<sup>22</sup> which is evaluated as a function of temperature by forcing agreement between calculated and experimental values of the bulk surface tension. The equilibrium droplet density profile that makes the work of formation an extreme value can be found by solving the following Euler-Lagrange equation:

$$\mu = \mu_0 - c\nabla^2\rho(r) \quad (6)$$

where  $\mu$  and  $\mu_0(\rho)$  are the chemical potentials of the bulk vapor phase and the homogeneous fluid at density  $\rho$ , respectively. Expressions for  $f_0$  and  $\mu_0$  are readily found from a given EOS. Cahn and Hilliard first found the reversible work of critical nucleus formation can be evaluated as:

$$W = \int [\Delta W + (c/2)(\nabla\rho)^2] dV \quad (7)$$

Here,  $\Delta W = W(\rho) - W(\rho_v)$ , and  $W(\rho) = f_0 - \rho\mu$ ,  $\rho$  is the density of the bulk phase. This GT form of work of formation may be used in Equation (3) to determine the nucleation rates. More details of implementing the GT to calculate the work of formation of critical nano-droplets can be found in references 11, 14, and 22.

### III. SAFT EOS AND COMPUTATIONAL APPROACHES

Chapman, et al.<sup>12</sup> proposed the first equation of state based on the statistical associating fluid theory (SAFT). They wrote the Helmholtz molar free energy  $F$  as:

$$F = F^{id} + F^{seg} + F^{chain} + F^{assoc} \quad (8)$$

where  $F^{id}$ ,  $F^{seg}$ ,  $F^{chain}$  and  $F^{assoc}$  are the ideal term, the segment term, the chain term and the association term, respectively. It is now referred to as SAFT-0<sup>23</sup> and we briefly summarized it in a previous work (14). The power of SAFT-0 EOS emerges from its key association term  $F^{assoc}$  for self-associating compounds which is given by:

$$\frac{F^{assoc}}{RT} = \sum_A \left( \ln X^A - \frac{X^A}{2} \right) + \frac{1}{2M} \quad (9)$$

where  $R$  is the universal gas constant,  $M$  is the total number of association sites on each molecule,  $X^A$  is the mole fraction of molecules not bonded at site  $A$ , and  $\sum_A$  represents a sum over all associating sites on the molecule. The mole fraction of molecules not bonded at site  $A$  can be calculated as follows

$$X^A = \left[ 1 + N_{Av} \sum_B \rho X^B \Delta^{AB} \right]^{-1} \quad (10)$$

where  $N_{Av}$  is Avogadro's number and  $\rho$  is the molar density of molecules, and  $\Delta^{AB}$  is the association strength, given as:

$$\Delta^{AB} = d^3 \left[ \frac{2 - \eta}{2(1 - \eta)^3} \right] \kappa^{AB} \left[ \exp \left( \frac{\epsilon^{AB}}{k_B T} - 1 \right) \right]. \quad (11)$$

Here,  $d$  is the effective temperature-dependent hard sphere diameter,  $\kappa^{AB}$  is the dimensionless association volume,  $\epsilon^{AB}$  is the association energy, and  $\eta$  is the segment packing fraction defined as follows

$$\eta = \frac{\pi N_{Av}}{6} \rho d^3 m \quad (12)$$

where  $\rho$  is the the molar density of molecules.

Evaluation of representing the association sites in water by four-site, three-site, and two-site models by Wertheim's thermodynamic perturbation theory (TPT)<sup>24,25</sup> shows that any of the models may be accurately applied, but the four-site model is difficult to apply for generalized analysis of multiphase equilibria. The two-site model is recommended by Suresh et. al.<sup>26</sup> because its accuracy is at least equivalent to that of the three-site model or four-site model, but it is more convenient to apply in general. Having drawn inspiration from the results of Wertheim's TPT and the recommendation of Suresh et. al., the two-site model of water ( $M = 2$ ) is chosen to be used in this work.

The effective temperature-dependent hard sphere diameter was adjusted in the SAFT-0 EOS to reproduce the water densities and the vapor pressures, particularly, for  $T < T_{max}$ .<sup>18</sup>

The temperature-independent sphere diameter  $\sigma$  was related, in the spirit of the Barker-Henderson theory<sup>27</sup>, to an effective temperature-dependent hard sphere diameter,  $d(T_r, m)$  as:<sup>12</sup>

$$d(T_r, m) = \sigma f(T_r, m). \quad (13)$$

Here,  $f(T_r, m)$  is a generic function of the reduced temperature,  $T_r = \frac{K_B T}{\epsilon}$ , by the Lennard-Jones intermolecular energy parameter  $\epsilon$ ,  $m$  is the number of segments per molecule, and  $\sigma$  is the temperature-independent segment diameter. For  $f(T_r, m)$ , Chapman et. el.<sup>12</sup> used a function similar to that fitted to the Lennard-Jones potential by Cotterman et. al.<sup>28</sup>,

$$d(T_r, m) = \sigma \left[ \frac{1 + 0.2977T_r}{1 + 0.33163T_r + f(m)T_r^2} \right] \quad (14)$$

where  $f(m) = 0.0010477 + 0.025337(m - 1)/m$  is just an abbreviation in terms of  $m$ . Although  $d(T_r, m)$  does not heavily change with  $T$ , it still can have a strong effect on the thermodynamics of the system, hence on the curves of the liquid-vapor coexistence. In this paper, an exponential adjustment to  $d(T_r, m)$  is introduced by adding a temperature-dependent term as:

$$d'(T_r, m) = d(T_r, m) + \sigma \lambda \exp \left[ -\alpha \left( \frac{T - T_{max}}{T_{max}} \right) \right] \quad (15)$$

where  $\lambda$  and  $\alpha$  are adjustable parameters that can be tuned for different water types and temperature ranges. The exponential form of the temperature-dependent effective diameter in Chen and Kreglewski work<sup>29</sup> where the Barker-Henderson integral equation<sup>30</sup> was solved using a square-well potential inspired us to use such form for adjustment. To explain further, this correction must quickly vanish for high temperatures ( $T > T_{max}$ ) where the  $d'$  resulting from Lennard-Jones potential works very well (even for water) and becomes the leading term below  $T_{max}$ . In order to fulfill this condition, the exponential correction depends on the reduced temperature  $\frac{T - T_{max}}{T_{max}}$  instead of  $\frac{K_B T}{\epsilon}$  (this correction quickly vanishes for high temperatures where the original  $d$  in eq.14 works very well).

The fitting parameters of our adjustment term for the two-site water model within temperature range (210 – 450K) are as follows:  $\lambda = 0.00805$  and  $\alpha = 7.53578$ . However, we already tested this adjustment for four-site ( $M = 4$ ) model of water in a different subject of study that will be published in the near future.

In this paper, we will apply the adjusted SAFT-0 EOS on water and follow the computational approaches in references (11 and 14) for CNT and references (14 and 22) for GT. The parameters for water were obtained by simultaneously fitting the experimental saturated vapor pressures and liquid densities<sup>18</sup> as given in Table I.

### IV. RESULTS AND DISCUSSIONS

The effect of  $T$ -adjustment on the temperature-dependent segment diameter is shown in Figure 1. The faster increas-

TABLE I. Regressed parameters of SAFT-0 EOS for two-site water.

$\sigma$ [Å]	$\varepsilon/k_B$ [K]	$m$	$\varepsilon^{AB}/k_B$ [K]	$\kappa^{AB}$
2.925	294.1	1.026	2938.8	0.053

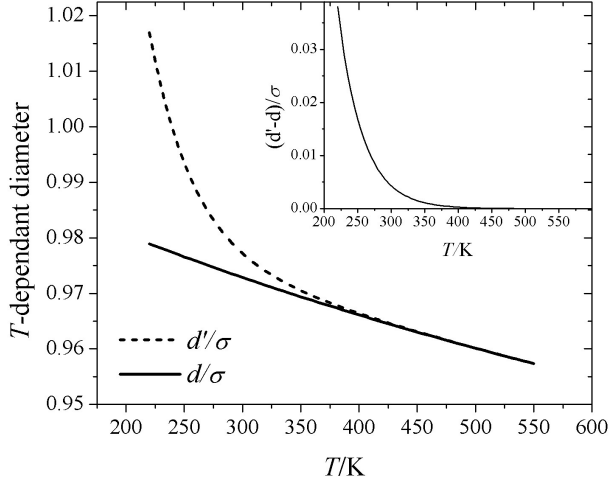


FIG. 1. Comparison between the temperature-dependent segment diameter  $d$  and the adjusted one  $d'$ . Inset: The differences between these two diameters represent the adjustment term vs. temperature.

ing of  $d'$  with decreasing  $T$  is the key point of this step which leads the anomalous behaviour of the supercooled water density. The inset shows the adjustment term in the temperature-dependent diameter  $d'$  with the temperature  $T$ .

Once the free energy density (Eqn.8) was established for two-site water model, it was fitted to the real water.<sup>18</sup> The predictions of SAFT-0 for the equilibrium vapor-liquid densities of water at different  $T$  compared to the experimental data generated using the IAPWS-95<sup>18</sup> are shown in Figure 2. Note that the results of the IAPWS-95 EOS may be regarded as the experimental values since this equation accurately treats the anomalous compressibility of supercooled liquid water and describes it to high precision. Starting with the results of regular SAFT-0 EOS, one can see that this equation predicts fairly accurately the equilibrium vapor-liquid densities for  $T > 335K$ , but it is severely deficient in predicting the anomalous liquid binodal line below  $T_{max}$  (dashed line). Later, we will see the projection of this misprediction on the determined nucleation rates of water. In order to resolve this weakness, a  $T$ -adjustment to the prerequisites ( $d'(T_r, m)$ ) of SAFT-0 EOS is necessary step because the experimental results are available below the freezing point, mainly in the ranges of  $220K - 260K$ .<sup>8</sup> This proposed adjustment makes fairly realistic prediction for the binodal lines (solid lines) of the supercooled water and the regular water within the temperature ranges shown.

Figure 3 compares accepted<sup>18</sup> binodal vapor densities and equilibrium vapor pressure of water in the temperature range 235 K and 450 K, in particular the range relevant for nucleation measurements. The water vapor density and vapor

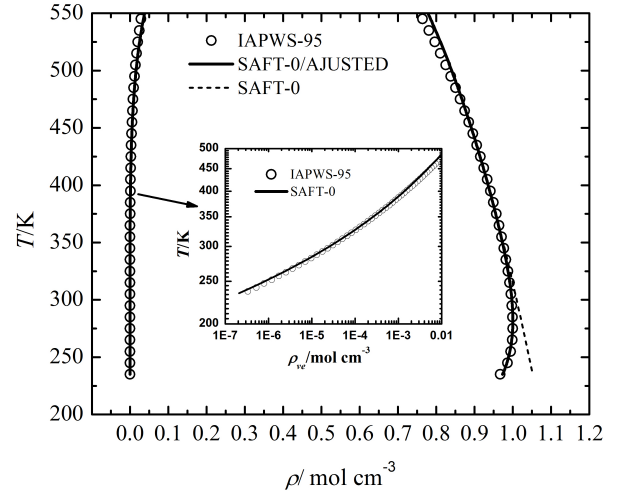


FIG. 2. Binodal densities of water calculated using SAFT-0 and SAFT-0/ADJUSTED compared with IAPWS-95 values.<sup>18</sup> Inset: Log-Plot of saturated vapor density vs.  $T$ .

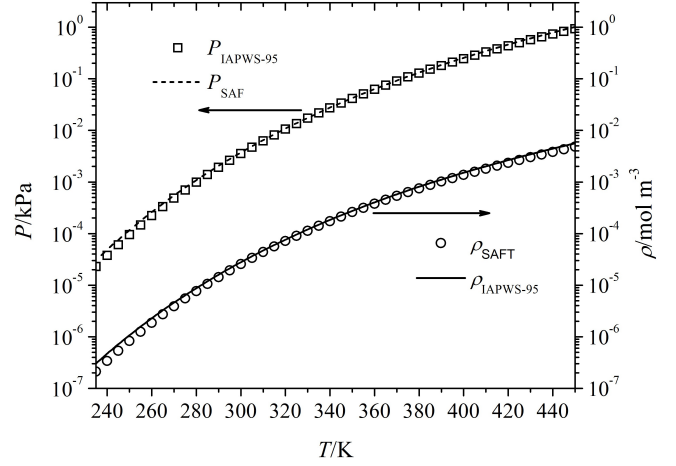


FIG. 3. Log. plot of saturated vapor pressure  $P$  and density  $\rho$  of water calculated using  $T$ -adjusted SAFT-0 EOS compared with IAPWS-95 values.<sup>18</sup>

pressure are well fit by the  $T$ -adjusted SAFT-0 EOS in this temperature range.

Both forms of the classical and nonclassical nucleation theories have been used with the SAFT-0 EOS to determine the nucleation rates of water. For comparison attempt, Fig. 4 compares the predicted nucleation rates of water using the SAFT-0 EOS (regular  $d$ ) with the experimental data<sup>8</sup> at five different temperatures. One can note that the GT and  $P$ -form fairly show a similar dependence on  $T$ , but the  $P$ -form has a slightly better  $S$  dependence and is roughly an order of magnitude higher than the GT. None of GT and CNT produces the  $J$  values very well.

Next, one can see in Fig. 5 that the nucleation rates using  $T$ -adjusted SAFT-0 EOS are very well predicted compared to

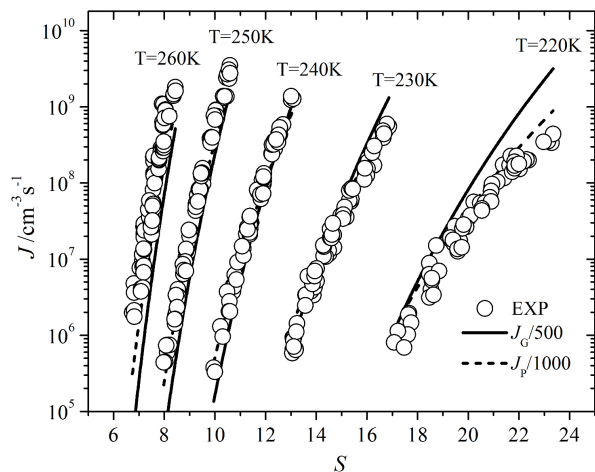


FIG. 4. Nucleation rates of water using the SAFT-0 EOS (unadjusted  $d$ ) with CNT and GT compared with experimental rates<sup>8</sup> at five temperatures.  $J_G$ : gradient theory;  $J_P$ :  $P$ -form of CNT.

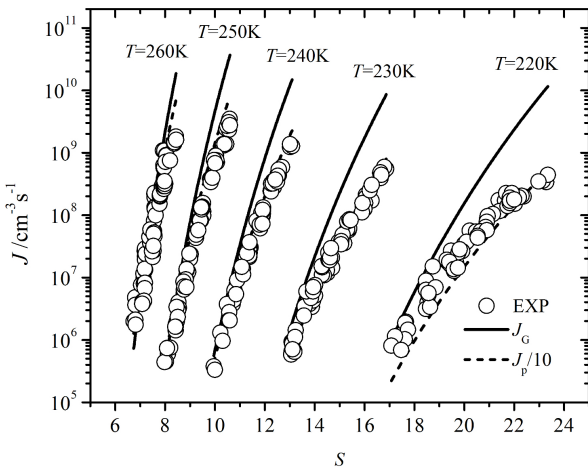


FIG. 5. Nucleation rates of water using the SAFT-0 EOS (adjusted  $d'$ ) with CNT and GT compared with experimental rates<sup>8</sup> at five temperatures.  $J_G$ : gradient theory;  $J_P$ :  $P$ -form of CNT.

the results in Fig. 4. First, the magnitudes of the nucleation rates are improved by factors of 500 and 100 for GT and CNT, respectively. Second, the  $P$ -form of CNT shows a slightly better  $S$  dependence and both have good  $T$  dependence. The  $P$ -form results are also roughly an order of magnitude higher than the GT and the experimental values.

Since the rate magnitudes of water from GT are better by a factor of 10 than those from the  $P$ -form of CNT and because the GT usually gives better results for other associating compounds than the CNT, its predictions of water rates will be used with Hale's scaled model for further explorations.<sup>15–17,31</sup> Hale's scaled nucleation rate equation is, perhaps, the most useful semi-empirical model that accurately describes the temperature dependence for many simple vapor systems and can be used to examine the accuracy<sup>14</sup>

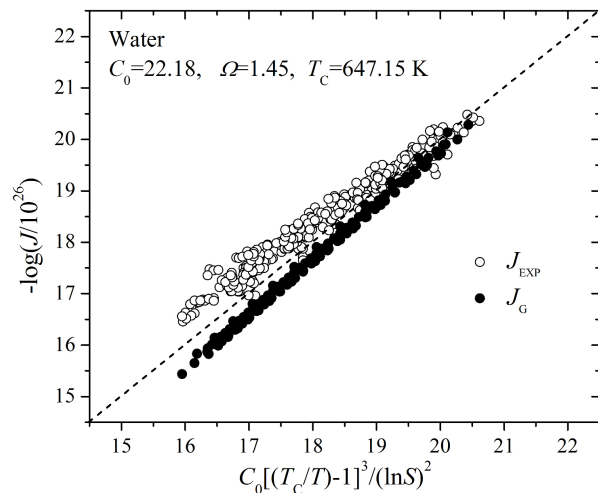


FIG. 6. Hale plot for the experimental nucleation rates of water<sup>8</sup> using the scaling factor  $C_0 = 22.18$ . The GT rates,  $J_G$ , calculated using the  $T$ -adjusted SAFT-0 EOS are also plotted.

of nucleation rate data. For example, the methanol nucleation rate data were corrected because they were influenced by the heat released due to small cluster formation during the vapor expansion<sup>32,33</sup> and these corrected data were assessed by Hale's plot in reference<sup>14</sup>. In a Hale plot, one plots  $\log J$  versus a quantity  $C_0[(T_c/T) - 1]^3 / [\ln(S)]^2$  that is essentially the dimensionless scaled work of formation.<sup>16,17</sup> Here,  $T_c$  is the critical temperature and  $C_0$  is a constant parameter related to the dimensionless excess surface entropy per molecule,  $\Omega$ , by the equation  $C_0 = (16\pi/3)\Omega^3 / \ln 10$ . Hale has found that for ordinary, that is, nonassociated liquids,  $\Omega$  values lie in the range 2-2.4, while for the associated liquids,  $\Omega$  is about 1.5.<sup>31</sup> Figure 6 shows a comparison of the water rates data and GT rates with the scaled nucleation rate mode,  $J_{scaled} = C_0[(T_c/T) - 1]^3 / [\ln(S)]^2$ . The value of  $\Omega = 1.45$  is in the range of that expected for polar substances. The magnitude of  $\Omega$  determines the slope but does not alter the temperature dependence<sup>31</sup>.

Hale plots provide a simple means of assessing the combined supersaturation and temperature dependence of a set of nucleation rates. For many systems, rate data from different laboratories often lie on or close to a single, universal line indicating their mutual consistency.<sup>34–37</sup> An application of the scaling that requires no knowledge of  $\Omega$  is shown in Figure 7 where  $\log J$  is plotted versus the scaled supersaturation.<sup>16</sup> The scaled supersaturation in Figure 7 is normalized with the factor  $(T_c/240 - 1)^{3/2}$  to keep the scaled supersaturation in the same range as  $\ln S$  in the traditional plot (Figure 5). One can see that the lines of data corresponding roughly to constant temperatures that spread out in a standard  $\log J_{exp}$  versus  $\ln S$  plot (indicated by the dot lines of the empirical fitting function) collapse onto a single line (data points indicated with open circles) when  $\ln S$  is scaled with  $(T_c/T - 1)^{3/2}$ .<sup>31</sup> Similar plot of  $\log J_{GT}$  versus  $\ln S_{scaled}$  demonstrates scaling of the predicted nucleation rates of water from GT (determined points indicated with filled circles). As expected,

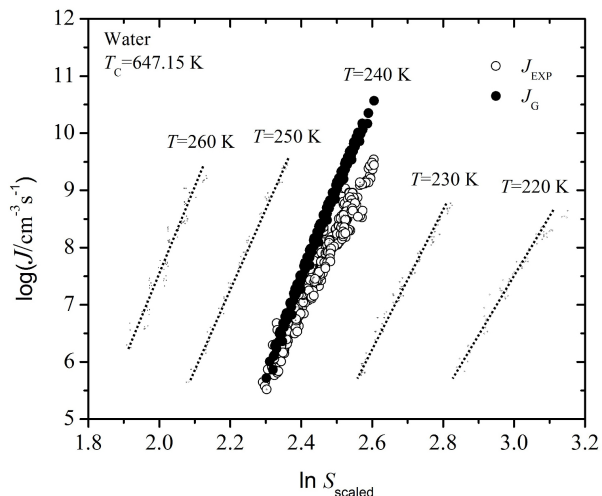


FIG. 7. The predicted homogeneous water nucleation rates from GT and the experimental values by Wölk and Strey vs. the scaled supersaturation function,  $\ln S / (T_c/T - 1)^{3/2}$ . The scaled supersaturation is multiplied by a normalizing constant,  $C_0 = (T_c/240 - 1)^{3/2}$ , so that the values fall in the same range of  $T = 240\text{K}$ . The dotted lines are guide lines of  $\log J_{exp}$  plotted versus  $\ln S$  (before scaling).

the GT results scale very well using Hale’s scaling model and show a good temperature-dependent agreement with the experimental data, but with slightly stronger dependence (larger slope) on the scaled supersaturation ratio  $S$ .

## V. CONCLUSIONS

We have used the SAFT-0 equation of state with the classical theory of nucleation (CNT) and non-classical gradient theory (GT) to determine the nucleation rates of water. In order to predict the water binodal lines with fair accuracy, its term of the temperature-dependent hard sphere diameter has been reformulated. This adjustment mainly aims to calculate the liquid binodal lines in some agreement with the experimental values,<sup>18</sup> particularly below the maximum density temperature where the liquid density anomalously decreases with decreasing temperature.

The calculated results were compared with experimental values<sup>8</sup> using a standard format. This  $T$ -adjusted SAFT-0 significantly improved the GT and CNT rates by factors of 500 and 100, respectively, as is seen by comparing Figs. 4 and 5. However, the  $S$ -dependence of the predicted values is slightly better in the CNT while the GT results are better by one order of magnitude. Interestingly, both give a good  $T$ -dependence and agree fairly well with the experimental values.<sup>8</sup>

In addition the GT results were compared with the water rates data using Hale plots. A Hale plot, in Fig.6, made with  $\Omega = 1.45$  ( $C_0 = 22.18$ ), shows that the GT rates scale

remarkably well. The scaling of the GT rates is most likely as a result of the accuracy of the  $T$ -adjusted SAFT-0 EOS that treats the effects of molecular associations. The nonclassical nucleation theory that avoids the unphysical assumptions<sup>1,11</sup> of CNT and provides improved treatment of the work of formation for small clusters also enhances the scaling of the GT results.

One can check experimental and theoretical nucleation rates without assuming a value of  $\Omega$  by using Hale’s scaled model of nucleation rates,  $J_{scaled}$ .<sup>16,17</sup> We plot  $\log J$  vs.  $\log J_{scaled}$  to examine both experimental and GT rates. We can see that the lines of data and GT rates corresponding roughly to constant temperatures that spread out in a standard  $\log J_{exp}$  versus  $\ln S$  plot collapse onto a single line when  $\ln S$  is scaled with  $(T_c/T - 1)^{3/2}$ . This remarkable scaling of GT rates is another confirmation of  $T$ -adjusted SAFT-0 EOS accuracy and its validity in determining the water nucleation rates.

In conclusion, SAFT-0 EOS with our  $T$ -adjustment of the temperature-dependent segment diameter is able to predict the thermodynamic properties of water in very good agreement with its experimental values, particularly in the temperature range below the maximum density point. We also conclude that except for a small deviation in the  $S$ -dependence, GT predicts the nucleation rates of water very well and its results scale nicely with two of Hale’s plots. These good results add another illustration of the fact that Hale plots can be used to assess theoretical results as well as experimental data.

Lastly, future computational studies of binary systems containing water and polar compounds are now expected to be more convenient and more accurate using our  $T$ -adjusted SAFT-0 EOS particularly two-site ( $M = 2$ ) compounds, such as alcohols.

## ACKNOWLEDGEMENTS

The author acknowledges Prof. Gerald Wilemski and Prof. Barbara Hale for valuable discussions and Dr. Abdalla Obeidat for sharing his GT code. He also acknowledges F. AlFaran and P. Field from HCT for their linguistic comments.

- <sup>1</sup>J. W. Gibbs, *The Scientific Papers of J. W. Gibbs. Vo. 1* (Dover Publications, 1961).
- <sup>2</sup>M. Volmer and A. Weber, *Z. phys. Chem* **119**, 277 (1926).
- <sup>3</sup>L. Farkas, *Zeitschrift für Physikalische Chemie* **125**, 236 (1927).
- <sup>4</sup>R. Becker and W. Döring, *Annalen der Physik* **416**, 719 (1935).
- <sup>5</sup>J. Frenkel, *The Journal of Chemical Physics* **7**, 538 (1939).
- <sup>6</sup>J. B. Zeldovich, *Zh. Eksp. Teor. Fiz.* **12**, 525 (1942).
- <sup>7</sup>S. Sinha, A. Bhabhe, H. Laksmono, J. Wölk, R. Strey, and B. Wyslouzil, *The Journal of Chemical Physics* **132**, 064304 (2010).
- <sup>8</sup>J. Wölk and R. Strey, *The Journal of Physical Chemistry B* **105**, 11683 (2001).
- <sup>9</sup>D. Brus, V. Ždímal, and J. Smolík, *The Journal of Chemical Physics* **129**, 174501 (2008).
- <sup>10</sup>D. W. Oxtoby and R. Evans, *The Journal of Chemical Physics* **89**, 7521 (1988).

- <sup>11</sup>A. Obeidat, J.-S. Li, and G. Wilemski, *The Journal of Chemical Physics* **121**, 9510 (2004).
- <sup>12</sup>W. G. Chapman, K. E. Gubbins, G. Jackson, and M. Radosz, *Industrial & Engineering Chemistry Research* **29**, 1709 (1990).
- <sup>13</sup>A. Obeidat and G. Wilemski, *Atmospheric Research 16th International Conference on Nucleation and Atmospheric Aerosols/ICSB 2004/16th ICNAA/16th International Conference on Nucleation and Atmospheric Aerosols*, **82**, 481 (2006).
- <sup>14</sup>A. Obeidat, M. Gharaibeh, H. Ghanem, F. Hrahsheh, N. Al-Zoubi, and G. Wilemski, *ChemPhysChem* **11**, 3987 (2010).
- <sup>15</sup>B. N. Hale, *The Journal of Chemical Physics* **122**, 204509 (2005).
- <sup>16</sup>B. N. Hale, *Physical Review A* **33**, 4156 (1986).
- <sup>17</sup>B. N. Hale, *Metallurgical Transactions A* **23**, 1863 (1992).
- <sup>18</sup>W. Wagner and A. Pruß, *Journal of Physical and Chemical Reference Data* **31**, 387 (2002).
- <sup>19</sup>R. C. Miller, R. J. Anderson, J. L. Kassner, and D. E. Hagen, *The Journal of Chemical Physics* **78**, 3204 (1983).
- <sup>20</sup>J. W. Cahn and J. E. Hilliard, *The Journal of Chemical Physics* **31**, 688 (1959).
- <sup>21</sup>J. S. Rowlinson, *J. Stat. Phys.* **20**, 197 (1979).
- <sup>22</sup>J.-S. Li and G. Wilemski, *The Journal of Chemical Physics* **118**, 2845 (2003).
- <sup>23</sup>S. P. Tan, H. Adidharma, and M. Radosz, *Industrial & Engineering Chemistry Research* **47**, 8063 (2008).
- <sup>24</sup>M. S. Wertheim, *Journal of Statistical Physics* **35**, 19 (1984).
- <sup>25</sup>M. S. Wertheim, *Journal of Statistical Physics* **35**, 35 (1984).
- <sup>26</sup>S. J. Suresh and J. R. Elliott, *Industrial & Engineering Chemistry Research* **31**, 2783 (1992).
- <sup>27</sup>J. A. Barker and D. Henderson, *The Journal of Chemical Physics* **47**, 4714 (1967).
- <sup>28</sup>R. L. Cotterman B. J. Schwarz J. M. Prausnitz, *AIChE J.* **32**, 1787 (1986).
- <sup>29</sup>S. S. Chen and A. Kreglewski, *Ber. Bunsen-Ges. Phys. Chem.* **81**, 1048 (1977).
- <sup>30</sup>J. A. Barker and D. J. Henderson, *J. Chem. Phys.* **47**, 4714 (1967).
- <sup>31</sup>B. N. Hale and D. J. DiMaggio, *The Journal of Physical Chemistry B* **108**, 19780 (2004).
- <sup>32</sup>R. Strey, P. E. Wagner, and T. Schmeling, *The Journal of Chemical Physics* **84**, 2325 (1986).
- <sup>33</sup>R. Strey, T. Schmeling, and P. E. Wagner, *The Journal of Chemical Physics* **85**, 6192 (1986).
- <sup>34</sup>M. Gharibeh, Y. Kim, U. Dierigsweiler, B. E. Wyslouzil, D. Ghosh, and R. Strey, *The Journal of Chemical Physics* **122**, 094512 (2005).
- <sup>35</sup>D. Brus, V. Ždímal, and F. Stratmann, *The Journal of Chemical Physics* **124**, 164306 (2006).
- <sup>36</sup>D. Ghosh, A. Manka, R. Strey, S. Seifert, R. E. Winans, and B. E. Wyslouzil, *The Journal of Chemical Physics* **129**, 124302 (2008).
- <sup>37</sup>D. Ghosh, D. Bergmann, R. Schwering, J. Wölk, R. Strey, S. Tanimura, and B. E. Wyslouzil, *The Journal of Chemical Physics* **132**, 024307 (2010).